This Dissertation

entitled

SOME TITLE

typeset with NDdiss2$_\varepsilon$ v3.2013 (2013/04/16) on May 31, 2017 for

Michael Thaddeus Moran

This LaTeX 2$_\varepsilon$ classfile conforms to the University of Notre Dame style guidelines as of Fall 2012. However it is still possible to generate a non-conformant document if the instructions in the class file documentation are not followed!

> Be sure to refer to the published Graduate School guidelines at `http://graduateschool.nd.edu` as well. Those guidelines override everything mentioned about formatting in the documentation for this NDdiss2$_\varepsilon$ class file.

It is YOUR responsibility to ensure that the Chapter titles and Table caption titles are put in CAPS LETTERS. This classfile does *NOT* do that!

This page can be disabled by specifying the "`noinfo`*" option to the class invocation.* (i.e.,`\documentclass[...,noinfo]{nddiss2e}`)

This page is *NOT* part of the dissertation/thesis. It should be disabled before making final, formal submission, but should be included in the version submitted for format check.

NDdiss2$_\varepsilon$ documentation can be found at these locations:

`http://www.gsu.nd.edu`
`http://graduateschool.nd.edu`

SOME TITLE

A Dissertation

Submitted to the Graduate School
of the University of Notre Dame
in Partial Fulfillment of the Requirements
for the Degree of

Doctor of Philosophy

by

Michael Thaddeus Moran

Manoël Couder, Co-Director

Michael C. F. Wiescher, Co-Director

Graduate Program in Physics
Notre Dame, Indiana
May 2017

SOME TITLE

Abstract

by

Michael Thaddeus Moran

The St. George recoil separator is currently undergoing its final commissioning work to fully characterize it ahead of the first experimental campaign to study (α, γ) reactions of astrophysical interest. The work currently completed to that end and comparison to the expected operation will be discussed. A single campaign utilizing the first two main sections of St. George to study two strong resonances in the $^{27}\mathrm{Al}(\mathrm{p}, \alpha)^{24}\mathrm{Mg}$ has been completed as an initial test of the combined angular and energy acceptance of th separator, the rejection properties of the Wien filter, and the exploration of the use of St. George for studying other astrophysically important reaction types. The results and comparison to accepted values will be presented alongside the extensions to other reactions and considerations for extending the analysis capabilities of the separator.

To Laura, my rock.

CONTENTS

FIGURES

TABLES

Your confusing thesis has captured my attention. Tell me more.

– Phil Hartman as Bill McNeill (Newsradio)

CHAPTER 1

INTRODUCTION

CHAPTER 2

EXPERIMENTAL SETUP

All experimental work was performed at the Nuclear Science Laboratory (NSL) at the University of Notre Dame, using the St. Ana 5U-4 accelerator and St. George. Commissioning work for the separator began in 2014 and is currently on-going (see Section 3.3). The experiment discussed herein consisted of three separate runs, each one week long, in December 2016 and February 2017. The first run tested a proposed close location for the detection system, the second run characterized the additional magnets required for a far location for the detection system, and the third run was the primary data collection run.

The accelerator provided a high intensity proton beam to St. George for the first and third runs, and a high intensity $^{4}He^{+}$ beam for the second characterization run. The 16-strip Si detector was installed at the two proposed focal planes (F_1 and F_2, see Fig. 2.1) to detect the produced α-particles from the $^{27}Al(p,\alpha)^{24}Mg$ reaction. Incident beam rejection was on the order of 10^9 for the first run and 10^{13} for the third run [CHECK THESE NUMBERS].

2.1 The St. Ana Accelerator and Transport Line

St. ANA (Strong Accelerator for Nuclear Astrophysics) is a 5 MV vertical, single-ended pelletron accelerator at the NSL, providing high-intensity stable beams to a number of experimental setups within a dedicated target room. The original designation of the accelerator by the manufacturer, National Electrostatics Corporation, was the 5U-4, denoting the five individual acceleration sections and the four charging

chains, causing the accelerator to commonly be referred to as the *5U*. Both names will be used interchangeably throughout this work.

The 5U, shown schematically in [FIGURE], accelerates a high-intensity ion beam produced by the Nanogen Pantechnik ECR source to the desired energy by energizing the terminal shell to high voltage. The acceleration tube, extending from the bottom of the shell to the bottom of the accelerator, steps that voltage down through a series of resistors and plates, creating an electric field gradient along the tube that accelerates the positively charges ion beam down and out of the accelerator. The beam is then bent around a 90°dipole magnet, called the analyzing magnet, and through a pair of vertical slits, called the analyzing slits, that provide energy identification of the beam. In addition, the current on the slits can be used as a feedback control system to regulate the voltage on the terminal shell when the accelerator is being run in "slit control mode," providing a highly stable beam with a small energy spread. A recently performed $^{27}\mathrm{Al}(\mathrm{p},\gamma)^{28}\mathrm{Si}$ resonance scan [4] was used to determine the beam energy spread of $\sigma_{\mathrm{beam}} \approx 0.3$ keV near a beam energy of $E_{\mathrm{beam}} = 1320$ keV. The 5U also contains focusing, directional, and diagnostic elements used to help tune the accelerator to provide a stable and well-behaved beam.

The transport beamline directs the analyzed beam to the desired experimental area through use of focusing and directional elements: two magnetic quadrupole doublets maintain a focused beam along the beamline; the magnetic dipole switching magnet directs the beam down one of the available experimental beamlines; and magnetic steerers shift and turn the beam within the beamline. The steerers act to maintain the beam along the magnetic optical axis of the quadrupoles and maximize the amount of beam being transported down the beamline from the accelerator. Sets of diagnostic equipment are also installed at various locations along the beamline to help monitor and restrict the beam, and the entire system is kept at a high ($\approx 8 \times 10^{-8}$ torr) vacuum through use of multiple turbomolecular pumps located

along the bealime.

The final section of the transport line is between the switching magnet and the entrance to St. George. This section of beamline prepares the beam to have the required characteristics at the target location. The final magnetic steerer is used to finalize the alignment of the beam, and the magnetic quadrupole triplet creates a small, well-focused beam at the target location.

2.2 The St. George Recoil Separator

St. GEORGE (Strong Gradient Electromagnetic Online Recoil separator for capture Gamma ray Experiments, henceforth simply *St. George*) is a recoil mass separator at the NSL [3] and one of the experimental beamlines accessible to the 5U. The design and operation is based on previous recoil separators (see [REFERENCES, DRAGON, ERNA, DRS, ARES]).

The separator consists of six dipole magnets, eleven quadrupole magnets, and a Wien filter. The separator was designed to accept recoils with a maximum energy and angular spread of $\Delta E/E = \pm 7.5\%$ and $\Delta\theta = \pm 40$ mrad, respectively, and to provide a mass separation of $m/\Delta m = 100$ and beam suppression of a factor $\geq 10^{15}$. At lower angular spreads, the transported ions may have a larger energy spread limited by the good field region within the third quadrupole Q_3. The design was guided by the desire to efficiently measure (α, γ) reactions with a beam mass up to $A = 40$ with high beam intensities and to fit the separator within the physical limitations of the target room at the NSL [3].

The separator is designed to transport recoils within a rigidity phase space relevant for measuring (α, γ) reaction cross sections, determined by the magnetic and electrostatic elements. The magnetic rigidity is defined as

$$B\rho\ [\mathrm{Tm}] = \frac{p}{q} = \frac{\sqrt{2mT}}{q}, \tag{2.1}$$

where p, q, m, and T are the momentum, charge state, mass, and kinetic energy of the desired particle, respectively. The magnetic rigidity defines the trajectory of the particle's movement within a homogeneous magnetic field of strength B along a circular path with radius ρ. Similarly, the electric rigidity is defined as

$$E\rho\ [\mathrm{MV}] = \frac{pv}{q} = \frac{2T}{q} \tag{2.2}$$

with the same variable definitions as before, and defines the circular trajectory a particle takes within an electric field of strength E. The limits for these rigidities are $0.1 \leq B\rho \leq 0.45$ and $E\rho \leq 5.7$ [3].

2.2.1 Subsections of St. George

The separator is divided into three sections, based on their purpose: the charge selection stage; the mass selection stage; and the clean-up stage. The stages are separated by the focal planes. Each of these stages will be discussed in turn. The layout of St. George is shown in Fig. 2.1.

The entire separator is tuned for a single $B\rho - E\rho$ rigidity, defined by the central energy of the recoils and its mass and charge state (see Eqs. 2.1 and 2.2). For commissioning purposes, a direct incident beam was used as a "test beam" to tune the separator without having to perform a reaction. The tuned particles will then travel down the central magnetic axis of the separator. Particles that differ in energy or angle from these central particles will travel through a different path (see Fig. 3.1).

The first section is the so-called *charge selection* stage, consisting of the first quadrupole doublet (Q_1Q_2) and the first dipole doublet (B_1B_2). The doublet Q_1Q_2 focuses the recoils through the dipole pole gap, and the doublet B_1B_2 provides the first rejection of beam due to the difference in magnetic rigidity from the desired recoils. At the first focal plane F_1, a single recoil charge state has been selected to

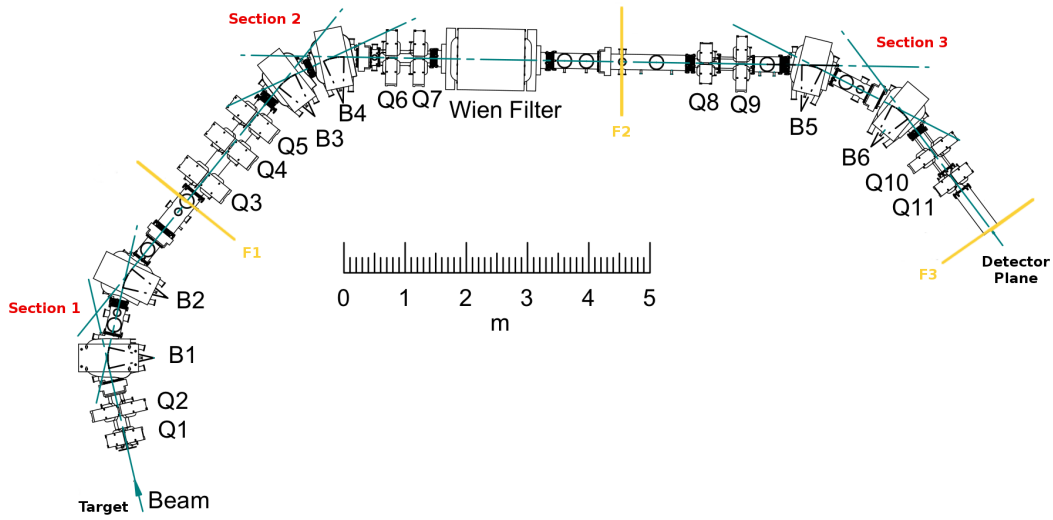

Figure 2.1. Layout of the St. George recoil separator. Quadrupoles are identified by Qn, dipoles by Bn, and focal planes by Fn. Section labels are placed near the dipole doublet within that section, and boundaries are the intervening focal planes. Adapted from Reference [3].

transport through the remainder of the separator. Horizontal slits may be placed at this focal plane to aide in the rejection of incident beam particles that have undergone a charge exchange event. Slits were not used during the commissioning work or during the primary experiment. At the end of this section, both beam and recoil particles are present within the separator.

The next section is the so-called *mass selection* stage, which contains the magnetic quadrupole triplet ($Q_3Q_4Q_5$), the second magnetic dipole doublet (B_3B_4), the second magentic quadrupole doublet (Q_6Q_7), and the Wien Filter (WF). This section's primary purpose is to reject the incident beam and create an achromatic focus at the second focal plane F_2. This focus is horizontally narrow at the focal plane to aide in the rejection of the beam. At this focal plane, a set of horizontal slits, called the mass slits, are placed to reject the remainder of the incident beam. The focused recoil particles will pass through the center gap between the slits. The mass

resolution of the separator depends on the particle distributions of the beam and recoil being focused and spatially separated at this position, and that the tail of the beam distribution minimally overlaps with the recoil distribution.

The Wien filter operates by having crossed electric and magnetic fields, oriented such that individually they would bend a particle beam in opposite horizontal directions, as shown in Figure [FIGURE]. From the beam's perspective, the electric field bends the beam to the right while the magnetic field bends the beam to the left. The fields are provided by a pair of electrostatic plates within the vacuum chamber and a magnetic dipole outside of the chamber. A Wien filter is set to allow for a single velocity to pass through the center of the element undeflected, according to $v = E/B$. For St. George, the Wien filter provides the final mass selection for our recoils, allowing the beam particles to be filtered out from the recoil particles, since the mass difference between the two ($\Delta m = 4$ when performing (α, γ) reactions) translates into a velocity difference.

The simplified description above is not entirely accurate, since our beam and recoils exist within a phase space envelope confined by ranges of allowed positions, angles, and energies. Since we inherently have an energy distribution of our recoils deriving from the convolution of the beam energy uncertainty with the target losses of the beam and recoils and the energy change arising from the γ ray emission, we do not have a mono-energetic recoil distribution passing through the center of the WF. When taken as a whole, the elements up to and including the WF create the proper beam and recoil properties to reject the incident beam based on their mass difference.

At this point, our beam envelope can be thought of as just our *recoil* envelope, where the particles still being transported through St. George are just those recoils produced in the reaction at the target location. In reality, the envelope still contains some beam particles, either through scattering off of the interior of the beam pipe,

diagnostic elements, or the residual vacuum, or through charge changing events with the residual vacuum [CITE]. Due to these factors, we cannot place the final detection system right after the Wien filter and instead need additional elements to further reduce the background.

This final section of St. George is the so-called *clean-up* stage, where the phase space of the recoils passing through the mass slits are matched with the phase space of the detection system, providing the last rejection of the incident beam particles. This section consists of, in order, a quadrupole doublet (Q_8Q_9), the last dipole doublet (B_5B_6), and a final quadrupole doublet ($Q_{10}Q_{11}$). These magnets transport the recoil particles that passed through the mass slits at F_2 through the detection system installed at the detector focal plane F_3. Since the detection system has a defined physical acceptance size, these magnets must reduce the physical extent of the recoil envelope within this space.

2.2.2 Diagnostic Equipment

To aide tuning the beam, additional diagnostic equipment has been developed and installed at various points along the separator. This diagnostic equipment can be divided between three basic types: Faraday cups, slits, and quartz viewers. These first two equipment types are present within other beamlines and the primary transport beamline, while the third was adapted for St. George based on principles encountered when working with other beamlines. The positions of this equipment is denoted in Figure [FIGURE].

Faraday cups are beamstops that also provide the user with the beam current being captured by the cup. The cup, shown in [FIGURE], consists of three main parts: the shield, the suppression, and the cup itself. This structure is attached to a linear motion drive, letting the cup be positioned in or out of the beam, and isolated from the beamline. The shield primarily protects the suppression from being hit by

incident beam but, due to its isolation, is also a point to read out the current and determine the physical extent of the beam at that point. Ideally, all of the beam would enter the cup portion, allowing the Faraday cup to determine the complete beam current at that location. Using the cup in this way as a tuning aide is possible since the cup locations were selected based on the beam optics properties, as those locations correspond to waist points of the beam. The suppression is necessary since electrons are emitted with energies in the rough range of $20 - 100$ eV when the beam strikes the physical cup. By biasing the suppressor to -300 eV, those electrons are directed back toward the cup, giving an accurate reading of the beam current actually hitting the cup.

Slits are an additional way to determine the passing beam current but also provide information about the spatial size of the beam. These slits are Ta plates attached to a linear motion, allowing the position to be controlled and determined from the exterior of the beamline. Each slit is isolated from the beamline, allowing the current hitting the slit to be read out at the console or to some other diagnostic program. The limiting factors for using these slits as a diagnostic device is their sensitivity, since unlike Faraday cups the slits used within St. George are not suppressed. The slits are then used as rough spatial diagnostics within the separator itself.

The quartz viewers used within St. George are divided between two types: an exterior quartz located at various exit ports, and an interior quartz that must be removed from the beamline. The locations of these camera systems are at the 0° exit ports of dipoles B_1, B_3, and B_5, the end of the detector chamber, and at focal planes F_1 and F_2. A schematic of one of the interior quartzs is shown in Figure [FIGURE]. The quartz are used for beam alignment and tuning the magnetic and electric elements of St. George, as explained in Section 3.3. When beam strikes the quartz material, the quartz fluoresces and the camera mounted immediately behind records the image and transmits it to the control console. Since this fluorescence is depen-

dent on the beam intensity, minimum currents of 200 nA are used to ensure that the beam shape can be accurately identified. Additionally, high intensity beams can melt the quartz material if left impinging on the system for extended periods of time, so maximum currents in the range of $1.5 - 2.5$ μA were used, depending on the actual beam particle selected.

2.3 Detector System and Data Acquisition

The full St. George detector system consists of a pair of microchannel plate based time-sensitive detectors and a single 16-strip Si detector for energy deposition. Combined, this detection system provides particle identification by way of the *Time of Flight vs. Total Energy* method. As residual beam particles can make it to the detector plane, either through scattering or charge exchange events, particle identification is required to provide final discrimination and beam suppression [CITE ERNA, DRAGON, DRS, etc]. As this experiment did not require the use of the full detection system, only the Si detector will be discussed further.

The Si detector is a Canberra PIPS (Passivated Implanted Planar Silicon) model PF-16CT-58*58-300EB, which has a detector area of 58×58 mm and is divided into 16 individual strips. The 16 strips allow for spatial resolution in one dimension, commonly taken to be the horizontal direction. For the experiment discussed herein, the detector was installed at focal plane F_2. Care was taken to ensure that the quartz viewer at that same location did not interfere with the operation of the detector.

The electronics for the experiment are relatively simple, needing only the energy signals from each of the 16 strips. A Mesytec MSCF-16 shaping filter amplifier provided amplification and signal shaping following the preamplifier, and a Caen V785 32-channel multi-event peak sensing ADC transformed those signals for the data acquisition system. Power to the detector was provided by Mesytec MHV-4 high precision bias supply unit, and was biased up to +40 V. Leakage current from

the detector during the run was ≈ 1.4 μA, but this high value was later shown to be due to the cable shielding internal to the beamline contacting the shielding installed to protect the detector when fully retracted. During the energy calibration runs where no detector shielding was present, the leakage current was ≈ 0.3 μA. The electronics used are the same as for a standard St. George experiment, allowing for an additional test of a subsystem of the full acquisition system. Data was recorded using the VM-USB crate connected to the St. George DAQ computer.

2.4 Target Chamber

The target chamber used for the commissioning work and the experimental campaign is different than that which will be used during a fully featured St. George experimental campaign, namely the Hippo supersonic helium gas jet target. Hippo will be used for (α, γ) experiments following the completion of the commissioning work. The specifics of that gas target are discussed elsewhere (see [6] and [8]) and will not be explored here further.

A commissioning target chamber was designed and built specifically for running the commissioning experiments and solid target studies. The chamber makes use of two of the turbomolecular pumps from the Hippo target to provide a high ($\approx 7 \times 10^{-8}$ torr) vacuum at the beginning of the separator and around the target location. The commissioning chamber consists of a pair of electrostatic plates within a rotating chamber, a target ladder, and a Faraday cup. The rotating chamber allows the combined target ladder and electrostatic plates to rotate through a range of $\approx 160^{\circ}$ (limited by the physical space around the target location) while maintaining a high vacuum, thus the target location does not need to be vented in order to change the angle of the target ladder and plates.

The electrostatic plates can be powered up to a maximum of 10 kV each from two single-phase high voltage power supplies and are operated remotely using an

Arduino-based controller. The properties of the plates (length, width, separation, etc.) were determined such that the produced electric field would be as homogeneous as possible within the limited space and provide a beam deflection of at least 40 mrad from the target location, within the physical limits of the chamber. Experimentally, deflections of 45 mrad have been achieved, allowing a full angular phase space sweep to be performed. Switching the polarity of the deflector plates must be done at the power supplies. Since the power supplies have a limited upper voltage, the maximum deflection for a test beam is limited by its electric rigidity $E\rho$. When not in use, the current striking the deflector plates could be monitored at the control console to use as an additional beam diagnostic.

The target ladder contains a 6.35 mm diameter collimator and a 2.06 mm collimator, separated by 11.1 mm. The large collimator is primarily used for mounting self-supporting solid targets, while the smaller collimator is primarily used for beam alignment and focusing purposes. The ladder is mounted on a high precision, manually controlled linear motion drive from [COMPANY]. The ladder may be fully removed from the beamline, and the central axis is aligned with the physical location of the jet target within Hippo. A thin Al foil was mounted for the experiment described herein.

The Faraday cup following the target chamber is an isolated FN-style cup, as shown in [FIGURE]. The back of the cup can be actuated open to allow beam to pass into the separator. From extended usage of the cup, the interior connection to the rear flap had degraded to the point that when open it was electrically isolated from the rest of the cup. If actuated while beam was hitting the cup, the flat would become charged and deflect the beam entering into St. George. To counter this effect, the cup preceding the target cup was placed into the beam before the target cup was removed. Since the commissioning chamber was designed to be temporary, this cup was not repaired or replaced following this discovery.

The Faraday cup allowed for beam with a maximum deflection of > 45 mrad to enter St. George, as measured using the deflector plates. This larger angular acceptance at the beginning of the separator ensured that the diagnostic equipment did not have a detrimental affect on the experiment and based the final acceptance at F_2 to be based on the specific tune of the separator. During some tests, the deflector plates were seen to intercept some of the beam when deflecting to 45 mrad, but since this value is again larger than the designed acceptance of St. George, this was deemed to not be detrimental.

CHAPTER 3

COMMISSIONING ST. GEORGE

The St. George recoil mass separator was designed to have an energy acceptance of $\Delta E/E = \pm 7.5\,\%$ and an angular acceptance of $\Delta\theta = \pm 40$ mrad, based on the kinematics of a set of astrophysically important (α, γ) reactions ([3] and Section 2.2). The total acceptance, i.e. the combined angular and energy acceptance, must be determined experimentally through direct beam studies, simulating reaction products with a degrading foil, or actually performing a reaction study. Recently, the energy acceptance was initially studied separately from the angular acceptance (published in [9]) to provide a relation between the predicted and experimentally determined field values. The angular acceptance was studied through a variety of methods, both in conjunction and without a corresponding energy acceptance requirement. Measuring the acceptance of a separator is paramount to using it for experimental measurements.

Two primary commissioning campaigns, determining the angular and energy acceptances for a given desired global setting of the separator, have been undertaken. The two global settings are: (i) the designed parameters for St. George for transporting heavy recoil products produced by (α, γ) reactions in inverse kinematics through the entire separator, and (ii) the altered parameters for transporting α particles produced by (p, α) reactions in forward kinematics to focal plane F_2. From each global setting, the separator elements can be scaled based on the desired transport particle's magnetic (Eq. 2.1) and electric (Eq. 2.2) rigidities. The experimentally determined values after scaling from the global setting may differ from the predicted scaled values when scaled over a large range, requiring multiple rigidities within the allowed rigidity

phase space to be explored to fully commission the separator. For the altered forward kinematics separator settings, due to the relatively small rigidity phase space the initial test reaction covers and the fact that a direct α beam can be used, the element field strengths were directly determined prior to the data collection experiment.

For the designed inverse kinematics separator settings, various beams spanning a large region within the desired rigidity phase space were used. Test beams included light beams (^{1}H and ^{4}He) due to their ease of production and heavier beams (^{16}O and ^{20}Ne) to simulate transporting heavy reaction products through the separator. Beam particle, charge state, and energy were limited by the capabilities of the 5U to produce the desired beam. The commissioning work was divided between focusing on the energy or angular acceptance relatively independent of the other. For some of the angular acceptance measurements, a small energy spread was included to better recreate the conditions under which St. George will be used.

3.1 Theoretical and Experimental Considerations

St. George was modeled within COSY Infinity (COSY-∞, henceforth *COSY*), a beam optics and transport language developed at Michigan State University [7]. The initial ion optics solution for the separator was calculated by Drs. Couder and Berg at the University of Notre Dame to maximize the angular and energy acceptance for a point-like target located prior to the separator. Optimization of the individual elements' properties allowed the separator to achieve the previously-stated energy and angular acceptances, create an achromatic focus at the mass slits (focal plane F_2), and transport all recoils to the final detector focal plane F_3 (see Section 2.2). Each magnetic element is represented by a single command within the code, defining the type and properties of the desired element. The three types of elements used within St. George—dipoles, quadrupoles, and the Wien filter—require different sets of values to be defined. The recoil envelope, consisting of a number of sample recoil

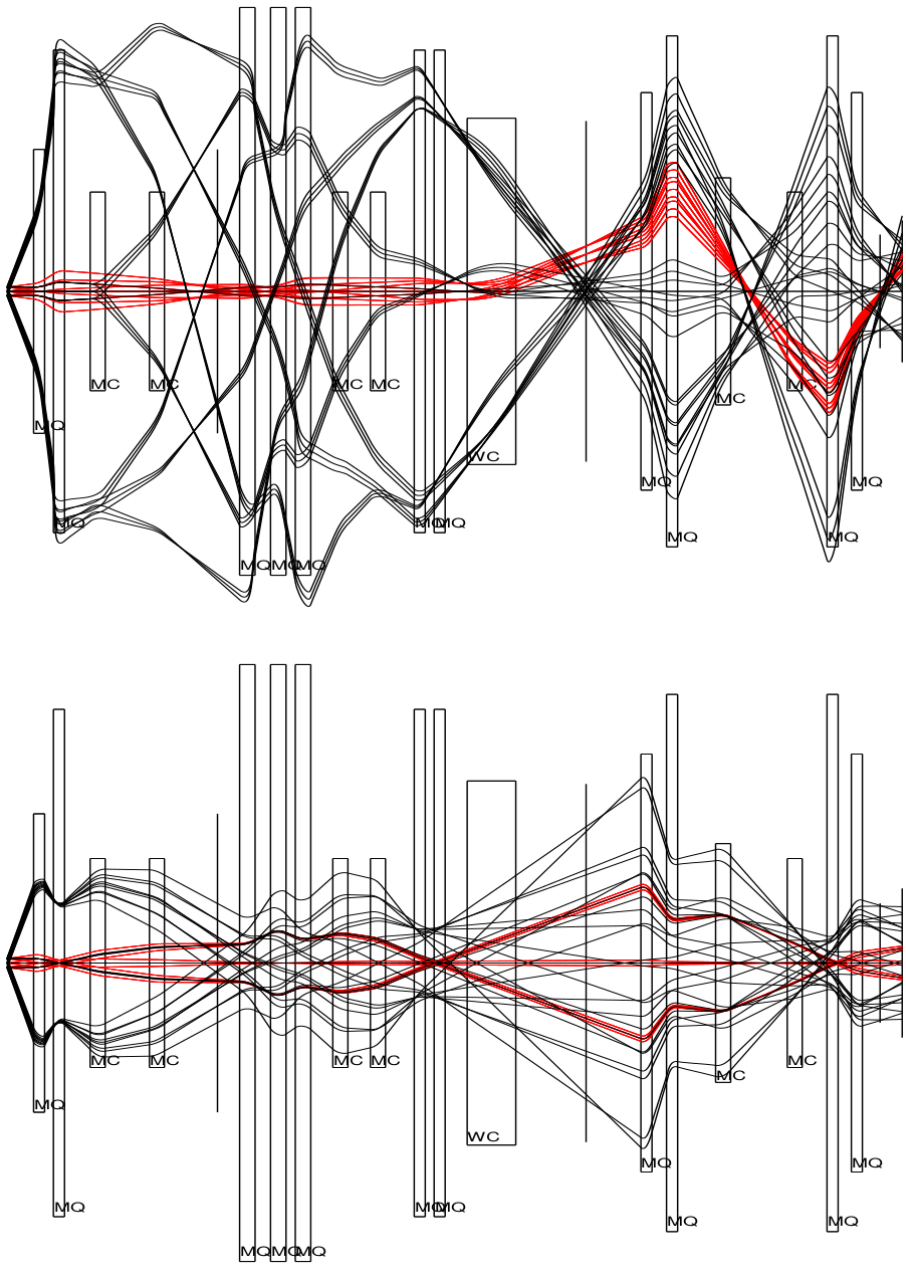

Figure 3.1. Horizontal (upper plot) and vertical (lower plot) rays through St. George. Recoil ^{41}Sc rays are shown in black and beam ^{40}Ca rays are shown in red. The beam rigidities are $B\rho = 0.331$ Tm and $E\rho = 2.907$ MV, and the recoil rigidities are $B\rho = 0.331$ Tm and $E\rho = 2.836$ MV. Both the beam and recoil are taken to be in the 11^+ charge state. The COSY calculation assumes that the recoil particles are spread within an acceptance range of $\Delta E/E \approx 7.5\,\%$ and $\Delta\theta = 40$ mrad. The transverse scale is highly exaggerated to show detail.

properties used as representative rays, for the final designed configuration is shown in Fig. 3.1. For the example shown, the quadrupole pole tip fields are given in Table A.1, where negative values represent a quadrupole focusing in the y-direction. The pole tip fields for (α, γ) experiments are for the test particles shown, while those for (p, γ) experiments are specific to this work (see Section [REFERENCE]). The actual fields used will depend on the rigidity of the desired particle to transport through the separator and can be scaled from these values.

The initial ion optics solution creates a transport map for particles passing through the entire separator that can be analyzed independently of the ray traces and provide the mathematical backing to the particles' trajectories within St. George. The transport map is dependent on the quantities

$$\begin{aligned} r_1 &= x & r_2 &= a = p_x/p_0 \\ r_3 &= y & r_4 &= b = p_y/p_0 \\ r_5 &= l = -(t - t_0)v_0\gamma/(1+\gamma) & r_6 &= \delta_K = (K - K_0)/K_0 \\ r_7 &= \delta_m = (m - m_0)/m_0 & r_8 &= \delta_z = (z - z_0)/z_0, \end{aligned} \tag{3.1}$$

where a and b are analogous to angles within each plane, δ_K is the energy difference from the desired energy K_0, δ_m is the mass difference from the desired mass m_0, and δ_z is the charge from the desired charge state z_0 [7]. The desired quantities are the values used to calculate the magnetic (Eq. 2.1) and electric (Eq. 2.2) rigidity, and thus set the fields of the elements within St. George, of the particle to be transported through the entirety of the separator. The time of flight difference l is not considered in analyzing the separator. The transport map contains terms up to fourth order.

The original ion optics calculation used default parameters to describe the fringe fields of the optical elements. A change in the shape of the fringe field can change the trajectory of the particles within the separator, as the total field that the particle

interacts with changes in magnitude. Since the fringe fields used to find the ion optics solution and those created by the actual magnetic elements within St. George may be different, the required field strength may also be different. The pole tip fields for a given particle rigidity, determined by the current setpoint for that magnetic, must be found experimentally, or a new ion optics solution using fringe field parameterizations that more accurately reflect those exhibited by the magnetic elements must be found.

This problem really only affects the focusing quadrupoles within the separator. While the dipole magnets are set based on the rigidity of the desired particle, those magnetic settings can also be determined by observing the trajectory within the separator itself. As the overall desire of the dipole magnets is to transport the desired rigidity down the center of the separator, diagnostic equipment aligned with this central axis can be used to ensure that the beam is traveling along this centerline. In doing so, the experimentally correct field setting for the dipoles can be determined without too much effort.

Setting the Wien filter can be done in a similar manner. The electric field strength is determined from the analyzed energy of the particle, the known charge state, and the desired bending radius of the filter. As these quantities are known to high or exact precision, the magnetic field can be set such that the particle trajectory continues along the central axis of the separator. The Wien filter was designed with magnetic yokes at the entrance and exit of the filter to restrict the magnetic fringe field so that it matches the electric fringe field created by the electrostatic plates, and those must be adjusted to their proper positions before the magnetic field can be set.

3.2 Separator Properties

The elements, power supplies, and supports were provided by Bruker Biospin and installed in 200X. The separator design requirements for the strengths of the optical elements were based on the maximum beam energy of the older KN single-ended Van

de Graff accelerator and the possible charge states produced by its internal ion source. The 5U and ion source have similar properties to this system. The power supplies for the magnets provide highly stable direct currents for each magnet individually, with $dI/I \approx 10^{-4}$ for the quadrupoles and $dI/I \approx 10^{-5}$ for the dipoles. The upper current limit is different for each magnet. The separator uses a robust water cooling system able to maintain the required 80 ± 2 °F magnet temperature for the entire system. The system is able to maintain the temperature even when all magnets are at their maximum currents for extended periods of time.

The Wien filter electrode power supplies are set separately based on their voltage, with voltage stability $dV/V \approx 10^{-5}$ in the range commonly used for experiments. The upper limits for these power supplies are ± 110 kV, with voltages below ≈ 70 kV used during previous work. The stability of the voltage is dependent on prior conditions within the vacuum chamber, requiring conditioning of the plates before higher voltages can be achieved. For voltages above ≈ 50 kV, the plates were conditioned to voltages at least 10 kV above the desired setpoint to provide a stable running condition. For lower voltages, no conditioning is necessary unless the vacuum chamber was recently vented (exposed to atmospheric pressure gases).

The properties (entrance and exit apertures, length, maximum field strength, good field region, etc.) were determined within the ion optics solution to transport the desired recoils, and built to match those specifications. The entrance and exit pole faces for the dipoles were designed to provide higher order corrections to the particle trajectory, since additional higher order magnets could not used [3]. Additionally, the shape of the Wien filter electrostatic plates were designed such that the electric and magnetic fringe fields were closely matched.

3.2.1 Magnetic Fringe Fields and Effective Field Lengths

Detailed two-dimensional magnetic field maps for multiple excitations of each magnet were provided by Bruker. The field maps allow a check on the good field region for each magnet and provide a description of the fringe fields. Field strengths at each location are measured in mT. The fringe fields for each magnet, excitation, and measurement radial distance can be analyzed separately if desired. From this data, the shape of the fringe field and the effective field length of the magnetic elements can be determined. As these values are essential to setting the necessary values for the quadrupoles, the analysis of the field maps focused on these elements.

A single edge fringe field is described by the Enge function given by

$$E(z) \equiv \frac{1}{1 + \exp\left[\sum_{i=0}^{N-1} a_i (\frac{-z}{D})^i\right]}, \tag{3.2}$$

where a_i are the desired expansion coefficients, D is the aperture diameter, and z is the longitudinal distance [1]. The formulation above is used within COSY to describe user-defined fringe fields. For a short magnet, which the St. George quadrupoles can be considered to be, the entrance and exit fringe fields are not completely independent of each other, since the fringe fields extend into the central region of the magnet. Instead of fitting each fringe field separately, we can instead fit the entirety of the magnetic field profile using a combined "short" quadrupole function, in terms of the Enge function, given by

$$k(z) = k_0 \left[E(L/2 + z) + E(L/2 - z) - 1\right], \tag{3.3}$$

where k_0 is a scaling parameter for the central field and L is the effective field length [1]. This formulation assumes a symmetric field profile, as both the entrance and exit fringe fields are modeled with the same Enge function. The effective field

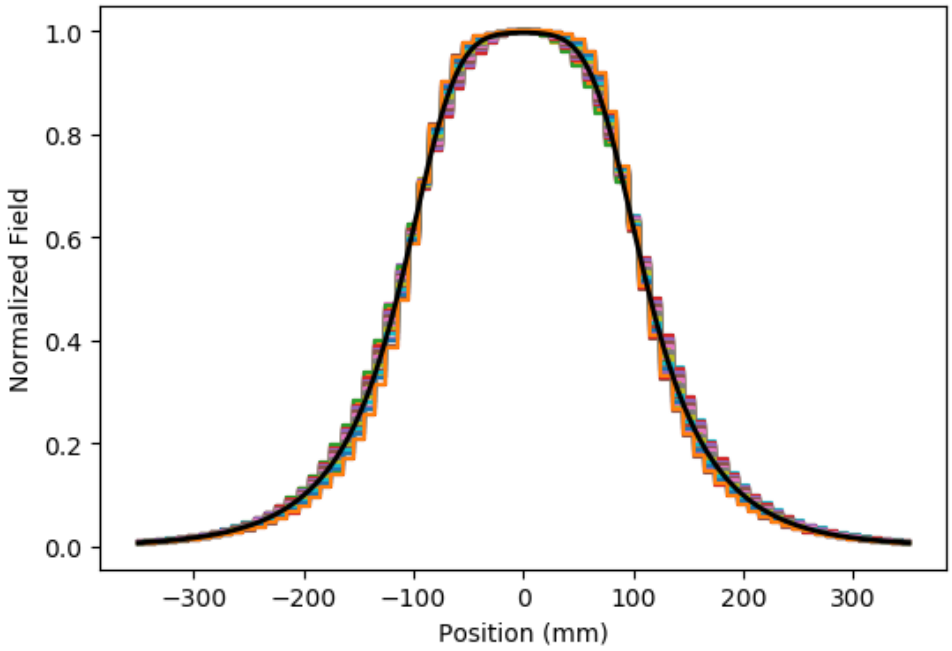

Figure 3.2. Normalized field and the resultant fit to the fringe field for the example quadrupole Q_{10}. The parameters of the fit are given in Table 3.1.

length, defined as

$$L = \frac{1}{B_0} \int_{-\infty}^{\infty} B(z)\,\mathrm{d}z, \tag{3.4}$$

where B_0 is the field strength at the center of the magnet, is the field length if the field were described with a pure "hard edge" or Heavyside function at the entrance and exit, i.e. no fringe fields.

Using the field maps provided by Bruker, we can determine the Enge coefficients and the effective field lengths for our magnets. For all calculations, since the field near the center of the magnet is relatively weak, the fields within 2 cm in the radial direction of the central axis were not used for determining either the effective field length or the Enge coefficients. Additionally, the effective field length and the shape of the fringe field were assumed to not differ with different magnet excitations, so all available data were used for each magnet at the same time. An example using Q_10

of the normalized fields used and the resulting fit is shown in Fig. 3.2.

The effective field lengths were calculated directly from the field maps by integrating along the z-direction for each radial distance provided. Since the maximum field strength for a given magnet current varies depending on the distance from the center, the individual "traces" of the magnetic field along the z-axis were normalized. This normalization is shown in Eq. 3.4 as the constant factor outside of the integral. The integration was performed using the Simpson's Rule routine provided by the SciPy Python package [5]. An average of these lengths was used. Differences between the calculated effective field length and those used within the initial ion optics solution were within 2 %. The new effective field lengths were used for all subsequent calculations.

Using the same normalized field "traces" along the z-axis, the Enge coefficients describing the shape of the fringe field may be determined. The field profiles at each radial distance were fit simultaneously. Using the default Enge coefficients as the initial parameter guesses, the summed mean squared error between the data and Eq. 3.3 was minimized using the Nelder-Mead downhill simplex minimization (see [11]) provided by SciPy. The additional factor k_0 was included in the fit, but is not needed when defining a fringe field within COSY. The process was repeated for each quadrupole separately. The updated Enge coefficients and their comparison to the default values used by COSY for $Q_1 0$ can be seen in Table 3.1, and the difference in the shape of the fringe field can be seen in Fig. 3.3.

In some cases, the field maps were not recorded far enough away from the center of the magnet for the fitting routine to converge, primarily due to the field not adequately reaching zero. In those cases, "dummy" points of zero field were pre– and post–pended to the individual "traces" at distances greater than 5 m from the center of the magnet to aide in convergence.

TABLE 3.1

ENGE COEFFICIENTS FOR Q_{10} COMPARED TO COSY DEFAULTS

Coefficient	Q_{10} **Values**	**COSY Defaults**
k_0	0.997 314 89	
a_0	0.372 552 61	0.296 471
a_1	6.186 997 78	4.533 219
a_2	−5.555 141 15	−2.270 982
a_3	6.962 108 51	1.068 627
a_4	−4.825 813 28	−0.036 391
a_5	1.313 578 7	0.022 261

The default COSY coefficients for the fringe field were compared against the data and shown to not adequately describe the field maps. The summed mean squared error when using the short quadrupole formalization and the default COSY parameters was significantly larger than that found through the minimization routine, and the difference was shown to be statistically significant. A visual comparison between the two models for Q_{10} is shown in Fig. 3.3.

3.3 Energy and Angular Acceptance

The energy and angular acceptances of St. George were determined experimentally through a series of experimental campaigns using multiple rigidities. The energy acceptance without a corresponding angular acceptance was shown to exceed the designed acceptance at zero degrees, with a measured energy acceptance of $\Delta E/E = \pm 8\,\%$ for ten different beam rigidities covering the phase space region for astrophysically important recoils [9]. The angular acceptance has been shown to meet

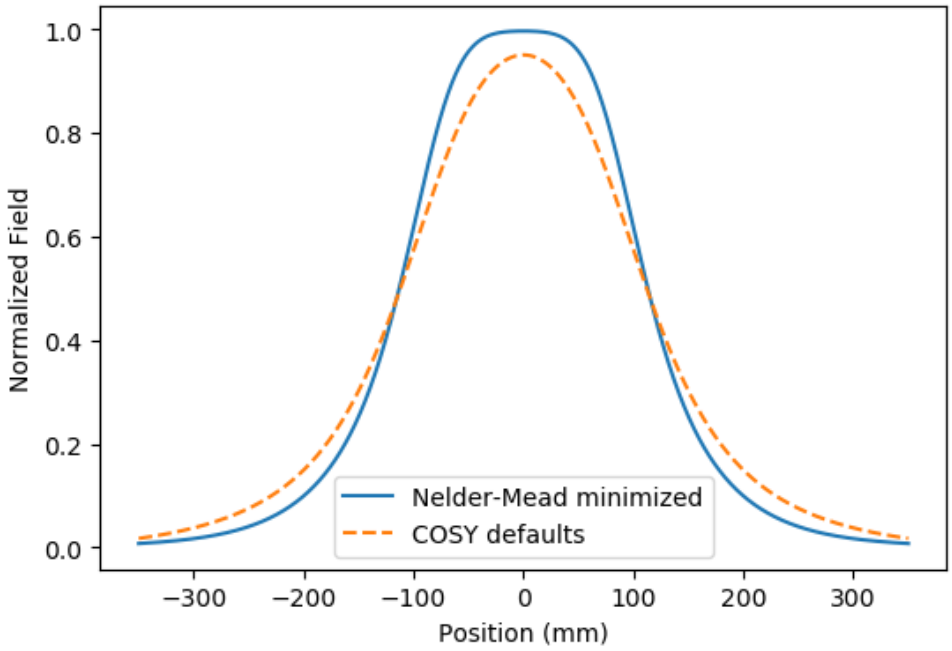

Figure 3.3. Comparison between fringe fields for the example quadrupole Q_{10}. The COSY default parameterization for the fringe field is the dashed orange line, and the fitted fringe field is the solid blue line. The distinct difference between the two field characterization requires the higher order effects arising from the fringe field to be taken into account.

the desired $\Delta\theta = \pm 40$ mrad in limited cases with an energy spread of $\Delta E/E = \pm 3\,\%$. The full total acceptance has not yet been measured within the designed phase space limits of St. George, with work ongoing.

Within the following discussion, the term "test beam" will be used in reference to an incident beam produced by the 5U with a desired rigidity. These test beams are defined by the beam particle, energy, and charge state selected by the operator and produced by the 5U. These beams were chosen for to provide particles with the desired rigidity and with beam currents in the range of $0.5 - 3$ μA in order for the diagnostic equipment to properly measure the beam. Additionally, those beams that commonly had highly stable 5U and ion source running conditions over extended times were selected to reduce beam preparation steps by the operators.

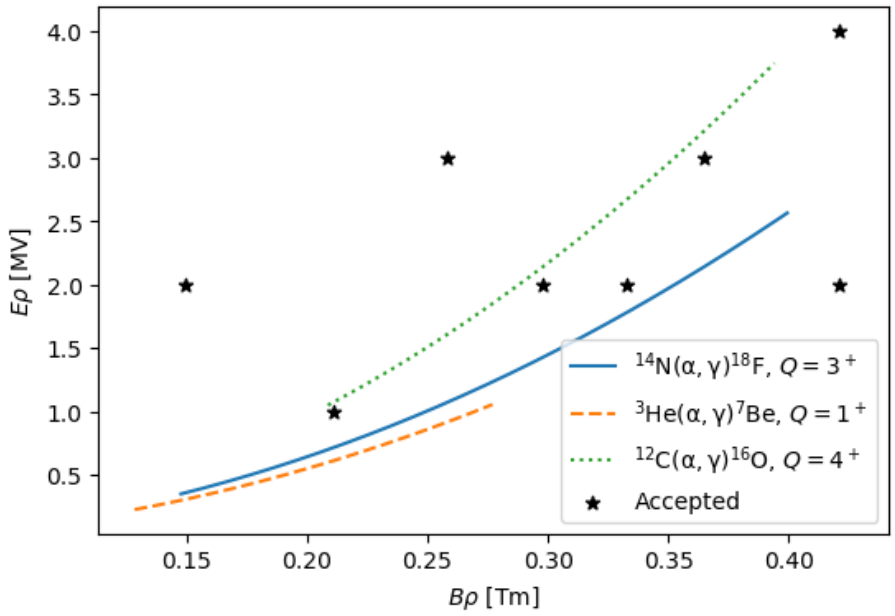

Figure 3.4. Designed $B\rho - E\rho$ rigidity phase space for St. George. Stars represent rigidities that have been shown to have the full $\Delta E/E = 8\,\%$ energy acceptance. Reactions shown are probable first experiments using St. George that use beam energies accessible with the 5U: ^{14}N at $E_{\text{beam}} \approx 0.7 - 5.0$ MeV (solid blue line), ^{3}He at $E_{\text{beam}} \approx 0.25 - 1.2$ MeV (dashed orange line), and ^{12}C at $E_{\text{beam}} \approx 3.0 - 10.0$ MeV (dotted green line). These energy ranges cover some of the astrophysically important ranges for the given reactions. Adapted from [9].

Acceptance measurements first probed the energy acceptance within the designed $B\rho - E\rho$ phase space. The rigidity phase space limits, along with measured acceptances and ranges for proposed future experiments is shown in Figure 3.4. While it is not possible to produce test beams with the 5U that completely span this phase space, the regions of astrophysical interest are accessible, and work focused on this region.

3.3.1 Beam Tuning and Properties

The commissioning runs followed a similar procedure for beam preparation using the 5U and the transport line. The beam rigidities were chosen to cover a region within the phase space limits of the separator that cover recoils produced through reactions of astrophysical interest. Both light (^{1}H and ^{4}He) and heavier (^{16}O and ^{20}Ne) beams were used to probe different regions of that phase space. Angular acceptance runs to date have only used lighter beams. The energy uncertainty of the beam is approximately 0.3 keV (see Section 2.1), and a conservative value of 0.5 keV will be used when necessary.

Beam preparation can be divided into two segments: preparing the $\Delta E = 0$ test beam to enter into St. George along the central magnetic optical axis, and transporting that beam along the central magnetic optical axis within St. George. The following procedures were used for all acceptance measurements, with differences being minor. The diagnostic equipment described in Section 2.2.2 was essential to performing the beam preparation steps and their use is highlighted below.

3.3.1.1 Before St. George

The test beam must meet simple requirements in order to be useful for commissioning St. George: it must enter St. George along the optical magnetic axis, and it must have a narrow waist point with a circular cross section at the target location. Additional requirements were shown to be beneficial experimentally: the focus must not be highly divergent, and the accelerator must be providing highly stable beam current with low energy uncertainty. The divergence of the beam was roughly known based on the focusing strength of the preceding quadrupole magnets required to provide the desired beam properties at the target location, with higher focusing strengths resulting in a more divergent beam. A rough sketch of this relation is shown in Figure 3.5.

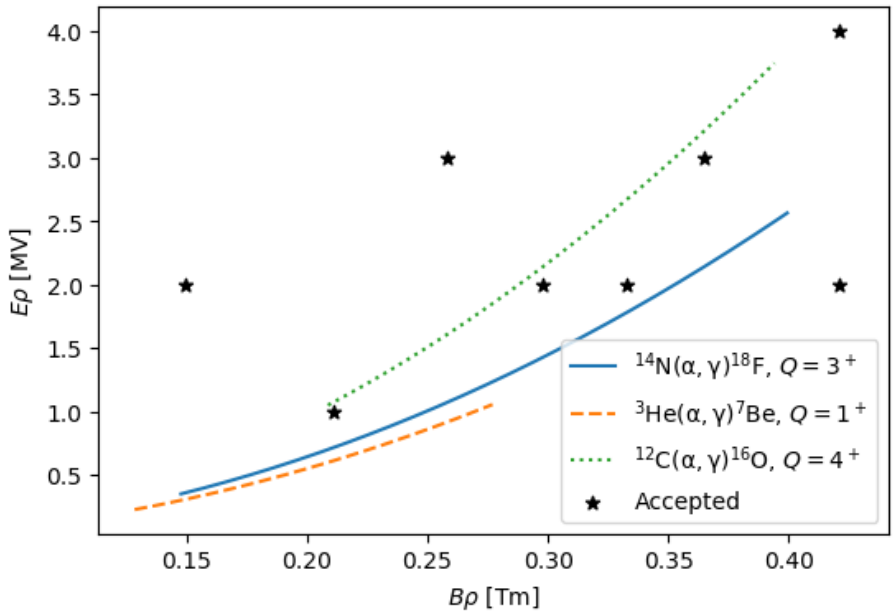

Figure 3.5.

The beam intensity is dependent on which diagnostic equipment will primarily be used. The isolated Faraday cups cannot read current below 50 enA when read through the logarithmic amplifier at the console, and the current can't be above 20-30 $e\mu$A as the cups are not currently water cooled and a high intensity and focused beam may melt some of the components. This upper current limit was not approached during the tests, since the cups were used in tandem with the quartz viewers. The quartz viewers are limited to beam currents of a maximum of 3-5 $e\mu$A, as higher currents risk heating up the quartz to a high enough temperature to cause them to shatter or melt. Since four of the quartzes are also barriers between the high (10^{-8} torr) vacuum within St. George and atmosphere, this limit must be carefully avoided. In practice, currents between 500 nA and 4 μA were used, based on the exact properties of the ion source for that particular run, the beam species, and the locations of slits on the primary transport line used to reduce the beam current.

The procedure for aligning the test beam to the magnetic optical axis is described

below. Major subsections of the procedure will begin with a short title in bold to guide the reader. The elements on the main transport line that may be necessary to adjust are the switching magnet with the X_6 steerer, and the Y_5 and Y_6 steerers (locations shown in Figure [FIGURE]). The steerers are labeled as such based on their position along the main transport line. Steerers X_6 and Y_6 are part of the same physical steerer but can be operated independently. Additionally, the quadrupole triplet directly before the target location will be necessary for final tuning.

Aligning the beam to St. George's optical axis: The desired test beam is transported down the St. George transport line and monitored with the Faraday cup at the target location, called the *target cup* for beam current stability. Diagnostic equipment before the target location are used as an aide to transport the beam and ensure that it has the desired properties. If necessary, the beam current is reduced. The quadrupole triplet is not be used at this point, since the beam may not be entering the element along its magnetic optical axis.

The beam is sent into St. George. With no field in Q_1, Q_2, and B_1, the beam hits the quartz viewer at the 0° exit port of the magnetic vacuum chamber, called the B_1 *quartz*. If the beam does not strike the quartz, then the final set of steering elements needs to be adjusted to send the beam into the quartz. When using the angular deflection commissioning chamber, the current readbacks from the plates provides an additional diagnostic on the trajectory of the beam.

Checking for steering: Quadrupoles Q_1 and Q_2 are adjusted independently of each other, and the resulting motion of the beam on the quartz is recorded. If the beam is aligned with the central magnetic optical axis of either quartz, the quadrupole will only focus the beam and not shift its position on the quartz, i.e. the spread in the beam will change but not its central position. The two quadrupoles must be adjusted independently of each other as any induced steering from a beam misalignment in one may be counteracted by a misalignment in the other quadrupole. If the beam

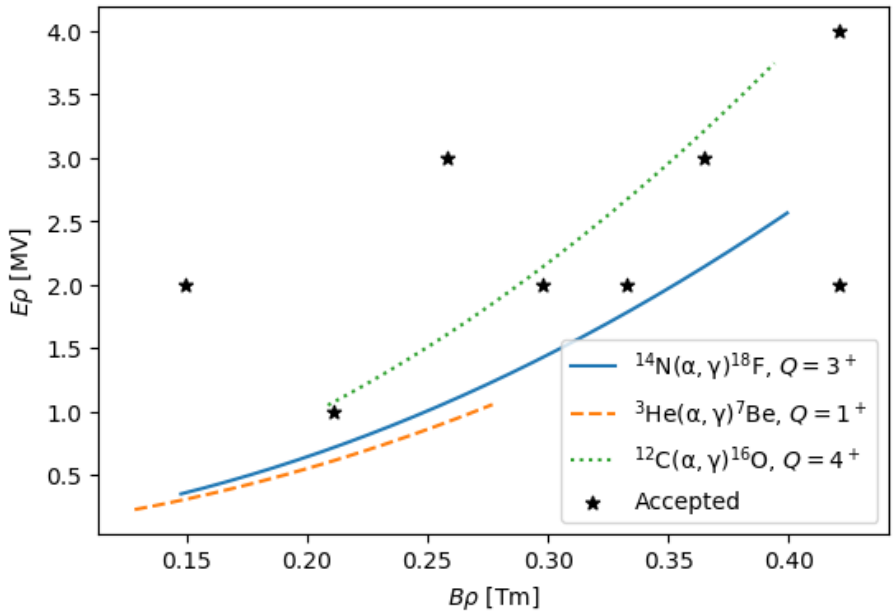

Figure 3.6.

is steered by either quadrupole, the steering elements corresponding the the focus direction of the offending quadrupole (Y_5 and Y_6 for Q_1, the switching magnet and X_6 for Q_2) are adjusted to reduce the amount of steering by that quadrupole.

A quadrupole steers a beam when the beam enters the magnetic element misaligned with the optical magnetic axis. Assuming that the element is brought from zero to defined strength, the focal length of the quadropule changes from ∞ to a length f. The effect on the beam is that those regions of the beam away from the optical axis are brought to pass through this focal point. When a beam is aligned with the optical axis, there is an equal amount of the beam on either side of this optical axis, so the beam spot will narrow along the focusing axis of the quadrupole. The beam will also extend along the other axis. If the beam is not aligned with the optical axis, this beam motion to the focal point will be viewed as a lateral motion along the focusing axis of the quadrupole. A sketch of this effect can be seen in Figure 3.6.

The goal for adjusting the steering elements before St. George is to have each quadrupole induce no steering on the beam. In practice, each change to the steering elements either increases or decreases the amount of steering in the direction of that element. The crossover point, where the beam switches from steering left to steering right for example, can be used to restrict the possible phase space of steerer values, as the beam must have a zero deflection position between those two extremes.

While each direction should be independent of each other, if the beam is far from the magnetic optical axis, a single quad may induce steering in both directions. When minimizing steering in a single direction, say the x-direction, the other direction must also be checked frequently.

At the end of this process, the beam is not deflected when the field strength for either Q_1 or Q_2 is increased or decreased independently of the other quadrupole. The beam may be said to be entering St. George along the optical magnetic axis. Due to the short distance between the first quadrupole doublet and the B_1 quartz, it may be necessary to increase the sensitivity of the steering to ensure that we are as aligned as possible to the axis.

Increase sensitivity: The beam is then sent further into St. George, first to the B_2 quartz located within the beamline then the B_3 quartz. The steering of Q_1Q_2 is again checked in the same fashion as before. As these quartzes are located further from the quadrupoles, they give a higher sensitivity to steering affects from misalignment than just using the B_1 quartz at the trade-off that the the quadrupoles can only be set to lower field strengths. Since the quartz is further from the focusing elements, the same focusing strength will create a larger beam spot on the quartz viewer. This effect can be seen in Figure 3.6.

These additional checks require B_1B_2 to have field. While these two dipoles must have an exact field strength when performing acceptance measurements or an experiment, at this point their fields only need to be coarsely set such that the beam

strikes the desired quartz. While the higher order corrections from these magnets do play a role in the direction and focusing of the beam, that contribution has no effect on determining beam alignment within the quadrupoles.

The steering elements are adjusted in the same fashion to minimize steering in Q_1Q_2. Since this steering was minimized during the previous step, these adjustments should be minimal. It may be necessary to have a weak field in B_3 in order to see the beam on the B_3 quartz, due to possible machining misalignments of the port that the quartz is attached to and the residual magnetic field within the dipole.

Include the quadrupole triplet: As the last focusing element before St. George, the quadrupole triplet (henceforth simply the *triplet*) is the final adjustable element to determine the beam properties when entering the separator. The triplet is used to focus the beam to a small spot at the target location, a requirement for both experiments and acceptance measurements. As it and Q_1Q_2 should lie on the same magnetic optical axis, its steering must also be checked and minimized if its use is desired for the present experiment. It was not used in all cases as the coarse target focus provided by the previous quadrupole doublets on the main transport line were deemed sufficient.

Before moving the beam off of the B_1 quartz, the steering effects of the triplet must be characterized in the same fashion as Q_1Q_2. During the steering minimization steps, both the triplet and Q_1Q_2 must both be minimally steering before moving forward.

Due to minor misalignments between the triplet and Q_1Q_2, it is usually not possible to have all elements nonsteering at the same time. In these cases, the steering of Q_1Q_2 should take precedence while having the triplet minimally steering. While the steering of the beam prior to the target location is important, experimentally the steering of the individual elements within the triplet cancel or nearly cancel each other out when the triplet is minimally steering, reducing that problem.

At this point, the main transport line has been tuned to prepare a well-focused and well-aligned beam entering into St. George. These elements are not to be touched during the rest of the tuning process. The triplet, due to the possibility of it having minor steering effects, must also have zero field for the remainder of the steering checks, and will be turned on for the actual measurement.

3.3.1.2 Within St. George

Once the test beam has been aligned to enter the separator along the magnetic optical axis, it must also be aligned to the magnetic optical axes of all of the quadrupoles within the separator. This alignment is done using only the dipoles B_{1-6} and the WF. Any minor misalignment in the vertical direction should have been corrected during the previous steps, but there is the possibility that there will be vertical steering within the separator, both from that misalignment and effects from the dipoles and quadrupoles. Within St. George, this equates to the y-focusing quadrupoles ($Q_{1,4,7,8,11}$) potentially steering minorly in the vertical direction despite the best efforts of the operator. As there are no elements within St. George that could correct for this, the steering effect of these quadrupoles may not be able to be eliminated. The procedure for this second alignment is straightforward, as the only elements used to adjust the steering of the quadrupoles are the two dipoles immediately prior.

Tuning to the WF: With the beam striking the B_3 quartz, quadrupoles Q_{3-5} are checked for steering. The primary focus of these steering checks will be on Q_3 and Q_5 which focus in the horizontal plane. The magnetic fields within B_1B_2 are adjusted to make these quadrupoles non-steering or minimally steering. The field precision is on the order of 0.1 G, read back by the Hall probes.

Due to potentially small misalignments in the St. George quadrupoles in relation to each other, it is commonly not possible to have Q_{1-5} non-steering simultaneously (see [9]). In these cases, minimal steering can be achieved through Q_{3-5} when Q_1Q_2

are non-steering by adjusting B_1B_2. At this point, dipoles B_1B_2 are set to the value corresponding to the magnetic rigidity of the particle and to maintain the test beam alignment to the optical axis.

Dipoles B_3B_4 are brought up to their rough field value to send the beam through the WF and onto either the WF quartz or the B_5 quartz. The quadrupoles Q_{6-9} are checked for steering, adjusting B_3B_4 to minimize the steering. Since there is some residual magnetic field within the Wien filter, the electric field is brought up to compensate for this bending to keep the test beam along the optical axis through Q_8Q_9. The field required is calculated by determining the bending radius caused by the residual magnetic field and creating the equivalent bending radius in the opposite direction for the particle's $E\rho$.

As the beam envelope has expanded, it will be necessary to bring Q_{1-5} to their desired values in order to check the steering of the remaining quadrupoles. Since these quadrupoles have been shown to be minimally steering, their effect on the beam trajectory through remainder of St. George should be negligible. It may be necessary to have a weak field in B_5 in order to see the beam on the B_5 quartz for the same reasons as explained previously for B_3.

Setting the WF: For a test beam with $\Delta E = 0$ and $\Delta\theta = 0$, the elements within St. George will be set to transport this along the central axis based on the test beam's rigidity. Since the energy of the beam is well known and the charge of the beam is exact, the electric rigidity $E\rho$ is also well known. The electric dipole within the WF is set for this rigidity and held constant for the remainder of the tuning process.

The magnetic field is set similarly to the other dipoles: to minimize the steering induced by the next set of quadrupoles (Q_8Q_9). Since the test beam was aligned to the optical magnetic axes of this quadrupole doublet in the previous step, the WF magnetic dipole must return the beam to this orientation. Additionally, since the elements within St. George act to prepare the beam to be separated by mass by the

WF, the quadrupoles Q_{1-7} must be set to the values determined by the test beam's magnetic rigidity $B\rho$.

The magnetic field for the WF is read back using a Hall probe located on the pole face. The field can be set precisely and related to the fields in the other dipoles. Once the magnetic field is set such that Q_8Q_9 do not steer the beam, the full WF is set.

Tuning through the detector chamber: Dipoles B_5B_6 are set to their rough values based on the $B\rho$ of the test beam, sending the beam through the detector chamber and onto the last quartz, called the *detector quartz*. As before, due to the size and shape of the beam envelope, Q_8Q_9 must be set to the required values. The final two quadrupoles $Q_{10}Q_{11}$ are checked for steering, and B_5B_6 are adjusted to minimize that steering.

Since the test beam is traveling through the detector chamber, the entire detection system must be pulled out of the way of the beam. Magnetic shields have been placed below the MCP constructs to remove the effect of the magnetic fringe fields on the beam deflection [10]. Once $Q_{10}Q_{11}$ are non-steering, the test beam is fully aligned to the optical magnetic axis of St. George.

3.3.1.3 Collimator and Target Position

The 2 mm diameter collimator at the target location (see Section 2.4) is used for setting the triplet to the proper values. A narrow waist beam at the target location is a requirement to achieve the maximum angular and energy acceptance for St. George. With the collimator in place, the triplet is adjusted such that the beam transmission, defined as the ratio between the beam currents before and after the collimator as read by two separate Faraday cups, is maximized and ideally close to 100 %.

Since the target chamber may rotate around its central axis, it is possible for the location of the collimator to become slightly misaligned between runs. Additionally,

the triplet may induce some minor steering at the target location, potentially moving the focal point radially from the optical magnetic axis. The target collimator position is then not a fixed value but must also be tuned to maximize transmission. Once the collimator position is found, the target position is immediately known.

Rotation angles between -5 and $+25°$, where $0°$ is to the right from the beam's perspective, and extensions of $91 - 96$ mm of the mounted linear motion have been explored. Maximum transmission has been found for collimator positions within this range of rotation angles and extension distances for multiple beams, restricting the total possible search space for the collimator. Extensions of the target ladder of ≈ 94 mm, and rotation angles near $+10°$ are common "best positions" for the collimator.

For acceptance measurements, the collimator is used to create a focal point at the target location. Once the beam preparation is complete, it is retracted from the beamline. When a target is used as a degrader, the collimator position is used to determine the target position.

3.3.2 Energy Acceptance

The energy acceptance of St. George at $\Delta\theta = 0$ mrad was measured to be $\Delta E/e = \pm 8\,\%$ for ten different rigidities (see Fig. 3.4 and [9]). The measurements took place before the capability to measure the angular acceptance and will be remeasured as part of a total acceptance measurement campaign. Test beam rigidities were chosen to cover an adequate region within the designed phase space near the rigidities expected for recoils of astrophysical interest and based on the restrictions imposed by the 5U and ion source.

For a given set of field settings for a test beam at $\Delta E = 0$ that provide $100\,\%$ transmission between the target cup and a Faraday cup located within the detector chamber at focal plane F_3, the separator is said to accept an energy difference if

the test beam is changed to that different energy and still have 100 % transmission between those two cups. To state that St. George has an energy acceptance of $\Delta E/E = \pm 8\,\%$, a single set of fields for the elements within the separator transmitted 100 % of the test beam between the two cups when its energy was changed within that energy change.

The procedure for measuring the energy acceptance of a single rigidity is outlined below. The slits located at the post-WF focal plane F_2 were used to define a beam center. As the tune for a given recoil is supposed to be achromatic at this location, these slits were used as both a diagnostic on the path of the beam and a check of this requirement during the measurements. Note that the tuning process for these measurements did not make use of the in-beam quartz viewers at F_1 and F_2 since they had not yet been installed.

Initial setup: After tuning a beam along the optical magnetic axis as described in 3.3.1, all elements within St. George are at a given field. The dipole elements, including the WF, are not touched. The transmission between the target cup and the F_3 cup is measured. If the transmission is 100 %, the beam energy was changed. If not, then the quadrupoles were retuned to transmit 100 % of the test beam between the two cups.

Quadrupole retuning was done systematically to prevent over- or under-focusing the beam at any location within St. George. With the beam on the F_3 cup, each quadrupole was adjusted individually to determine what field is required to transmit 100 % of the beam to the cup. After finding that field, the difference is recorded and the quadrupole is returned to its original value. This process is repeated for every quadrupole acting independently. If a single quadrupole could not achieve 100 % transmission on its own, it was not included in the next step. Assuming N quadrupoles adjusted by ΔB_i to give 100 % transmission, the individual quadrupoles Q_i were changed by $\Delta B_i/N$. This approach usually resulted in achieving 100 %

transmission for the $\Delta E = 0$ case.

The quadrupole adjustment described was used at every step if the tune was shown to not transmit 100 % of the test beam. Previous settings of the quadrupoles were recorded to map regions of field strengths were 100 % transmission was achieved for different energy changes.

Changing energy: The beam energy was changed to $\Delta E/E = -8\,\%$ by changing the accelerator. The transport beamline was scaled automatically to account for the change in rigidity. The beam was shown to enter into St. George along the optical magnetic axis by putting the fields within Q_1, Q_2, and B_1 to zero and checking the steering of the first two quadrupoles. Since this energy change is minor, in most cases only the switching magnet needed to be changed. The magnets $Q_1 Q_2 B_1$ were brought back to their required values and transmission between the two cups was checked.

If the beam was fully transmitted to the F_3 cup, the settings for St. George were said to have an energy acceptance of $\Delta E/E = -8\,\%$. The beam energy was then changed to $\Delta E/E = +8\,\%$, following the same procedure, and transmission was checked. If the beam also was fully transmitted, the separator tune was said to have an energy acceptance of $\Delta E/E = \pm 8\,\%$ and the measurement was complete.

Where 100 % transmission was not achieved, the quadrupole scaling described previously was used. The new tune was recorded, and the beam energy was returned to $\Delta E = 0$ to check transmission. This process was continued until all three energy points had 100 % transmission for a single setting of St. George. During this cycling, referring to previous values was used to prevent correcting the tune in one direction at one energy only to change back to the previous tune at another energy.

Since the F_2 slits were placed around the beam center, achieving 100 % transmission was only possible if test beam had a nearly or completely achromatic focus following the WF, one of the requirements for normal operation of the separator.

Additional measurements: For subsequent energy acceptance measurements, instead of using the COSY predicted values, an energy acceptance tune scaled based on the magnetic rigidity $B\rho$ of the new test beam was used for the initial quadrupole settings. If the difference in $B\rho$ was sufficiently small, the required adjustments to the quadrupole fields were minimal, speeding up the measurement process. As more individual energy acceptance measurements were made, the scaling based on $B\rho$ became more robust to slight differences in beam preparation and species.

Once the ten rigidities within the astrophysically interesting phase space of the separator were measured, work moved to measuring the angular acceptance.

3.3.3 Angular Acceptance

As of this writing, the angular acceptance of St. George has been measured to be $\Delta\theta = \pm 40$ mrad in the horizontal and vertical planes for a single rigidity. The acceptance was shown by ensuring 100 % transmission when deflecting the beam 40 mrad in each direction, and quadrupole adjustments followed the same procedure as during the energy acceptance measurements. The measurement was done without a corresponding energy acceptance, and without the requirement that the test beam be focused at the focal plane F_2 following the WF and without the beam passing through the slit opening at that location for all deflection angles. The measurement was then a single "proof of concept" that an angular acceptance could be measured using the new diagnostic and control equipment installed. Due to complications with the measurement process, multiple attempts at measuring the angular acceptance, each with a different procedure, were tried. These attempts are outlined below.

Deflector plates only: A test beam is tuned to provide a non-steering beam with 100 % transmission between the target and F_3 cups. The deflector plates (see Section 2.4) are rotated so that they deflect the beam in a single plane. The horizontal plane was commonly chosen first. Since the entrance aperture for the target cup is

larger than 40 mrad, it does not intercept any of the beam when it is deflected. Angles between 0 and 40 mrad were used and the current on the F_3 cup was monitored. The maximum angle that provided 100 % transmission was recorded.

If the maximum angle achieved was not 40 mrad, the quadrupoles were tuned in the same fashion as for the energy acceptance measurement but with the deflector plate set to an angle greater than was accepted such that the beam is still partially captured by the cup. The changes to the quadrupole fields were recorded, and all quadrupoles that could provide 100 % transmission were scaled to new values. The beam was returned to $\Delta\theta = 0$ to ensure that the new tune still provided 100 % transmission in this case, and the deflection was changed.

A single plane was checked for ±40 mrad first before switching to the other plane, and any retuning was done to also transmit 100 % of the beam to the final cup. The deflector was also rotated to check the other plane, and the quadrupoles retuned to provide 100 %. In general, this procedure did not provide 100 % transmission when deflecting a test beam up to 40 mrad in the four cardinal directions. This procedure was used for the single full angular acceptance measurement.

Additionally, since the angular and energy acceptance is dependent on the beam extent and shape at focal plane F_2, the WF quartz was used to aide in tuning Q_{1-7} to their proper values. The beam should move minimally at this location when deflected up the the maximum 40 mrad in any direction. The beam profile is required to be horizontally narrow for the highest mass separation, requiring the vertical extent to be large. Using this intermediate quartz slightly improved the ability to tune the separator but did not allow for a full angular acceptance measurement to be performed.

Degrader foil: The limiting factor in using the deflector plates as the only angular change is that each direction must be looked at independently. Assuming the plates are aligned to deflect in the horizontal direction, only one direction (left

or right from the beam's perspective) can be viewed at a time without some manual adjustment to the deflector plate power supply. The cyclic problem of correcting the beam trajectory only to remove that correction becomes harder to avoid. Since the plates can only deflect along a single plane, the additional unknowns of removing a large angular acceptance along a difference by making changes on the current plane also decreased the possibility of success.

At the target location, Al foils of different thicknesses were placed to degrade the beam, creating a spread in angle and energy at the same time. Foil thicknesses were matched with beam properties to fall within the anticipated $\Delta E/E = \pm 8\,\%$ and $\Delta\theta = \pm 40$ mrad acceptances of St. George. Since the foils also induce an energy loss for the test beam, the separator dipoles needed to be properly scaled down to the correct values after the test beam (without foil in place) was aligned to the magnetic optical axis. The scaling required accurate and precise measurements of the foil thicknesses. Thicknesses ranged from $100 - 250$ μg/cm^2, and ^{1}H and ^{4}He test beams in the energy range of $0.9 - 2.0$ MeV were used.

Using the WF quartz, the test beam was tuned to have the correct phase space properties at F_2. The degraded test beam is emitted into the separator within a phase space determined by its interaction with the foil, allowing the magnets to be tuned without relying on the slow change between deflection angles and directions and including the minor energy acceptance measurement. Currently, no full angular acceptance measurements have been made past F_2.

Reaction Measurement: Additional measurements have been made of the angular acceptance with an energy acceptance and a nearly achromatic focus at the F_2 focal plane. These measurements were for the altered settings for transporting α particles from (p, α) reactions. The measurements are a different "proof of concept" for the angular acceptance measurements by verifying a $\Delta\theta = \pm 40$ mrad acceptance with the deflector plates before using a foil to produce the full angular spread. In this

case (see [SECTION]), the transported particles are the reaction product α particles, verified using a direct test beam of $^4He^{2+}$. The transported reactions products within the $\approx$ 45 mrad cone limited by the target Faraday cup were transported to F_2 and detected with the Si detector.

3.4 Considerations

Full acceptance measurements require a fine detailed understanding of the operation of St. George. Previous work has provided the initial understanding on providing a large energy acceptance of at least $\Delta E/E = \pm 8\,\%$ and angular acceptances near $\Delta\theta = \pm 40$ mrad. Combined measurements have been limited to a large energy acceptance and small angular acceptance or vice versa. Current work is ongoing on providing an improved understanding of the operation of St. George, particularly in setting the quadrupole fields.

A full commissioning of the separator system requires the gas target, separator, and detection system to be operated in parallel and well-understood. The current status of each of these discrete systems is varied. The Hippo gas target has been tested in a prior configuration, and work has been started to redesign the upper chamber to improve the possibility for monitoring incident beam current and using a γ detector in coincidence with the final detector system. The combined $E_{\mathrm{TOTAL}} vs. TOF$ detection system has been shown to work for test surface sources. Silicon detectors are known to be very robust, and the Si detector and acquisition system has been used for a successful measurement with St. George for (p, α) measurements. The separator status has been explored earlier in this chapter. Final verification of the separator will be measuring the test reaction $^{14}\mathrm{N}(\alpha, \gamma)^{18}\mathrm{F}$ in inverse kinematics.

CHAPTER 4

MEASURING THE $^{27}\mathrm{Al}(\mathrm{p},\alpha)^{24}\mathrm{Mg}$ CROSS SECTION

Alphas have more mass because they spend so much time at the gym getting swole.

– Laura Moran

An experimental campaign to study the $^{27}\mathrm{Al}(\mathrm{p},\alpha)^{24}\mathrm{Mg}$ reaction with the St. George recoil separator was undertaken at the NSL. Runs were completed in December 2016 and February 2017, with runs focusing on determining the correct magnetic fields within St. George completed in Fall 2016 and February 2017. Two low energy resonances were measured with beam currents in the $2-3$ μA range in February 2017.

The first portion of these runs fall under general St. George commissioning work as discussed in Chapter 2 and will not be repeated here. The second portion of the runs involved characterizing the target and the detector, finalizing the optimal settings for the separator, and performing the experiment. The reaction of interest produces α particles in the energy range of $2-3$ MeV for the desired proton energy range. Resonance properties were determined and compared to predicted results from the R-matrix formalism.

The experiment was devised as a way to verify some of the acceptance properties of St. George *in situ* and as a proof-of-concept for studying (α,γ) reactions across a wide range of targets and energies. Additional work was done to try to observe the (α_1,γ) channel, but due to the kinematics of this case, it was not observed with a low enough beam background at the detector.

4.1 Altered Tune

The magnet settings for St. George were determined to transport α particles with a minimal energy spread within the full 40 mrad acceptance cone to the F_2 focal plane after the Wien filter. Additionally, the first two sections must match up the phase space of these produced produced particles to the Si detector. For experiments using the entirety of St. George, this phase space matching is done by the final section, with the first two sections providing charge and mass selection. The beam spot at F_2 for these studies maximizes this requirement by having a narrow (within the dispersive x-plane) and tall (within the y-plane) physical beam spot at F_2. The requirements on the beam spot for measuring (α, γ) reactions at this focal plane require an approximately symmetric spot size in both directions and one that is smaller than the physical face of the detector. For these reasons, an alternate tune for St. George needed to be devised to achieve these desired beam properties.

The initial COSY code for St. George (see Section 3.1) was altered to model the shortened separator and provide information on the beam characteristics at the new detector focal plane. The magnetic field settings for the seven quadrupoles Q_{1-7} were adjusted to transport the recoil particles to the detector plane with a final beam spot no larger than the face of the Si detector of 58×58 mm. Final pole tip fields are given in Table A.1.

The smaller energy spread of the produced α particles allowed for a

4.2 Experimental Considerations

4.2.1 Beam Reduction

Incident proton beam reduction on the order of $10^{10} - 10^{14}$ are required to avoid damaging the Si detector and observing off-resonance yields of the produced α particles. These limits are within the designed capabilities of St. George but must be

verified experimentally

4.3 Procedure

The procedure for performing the $^{27}\mathrm{Al}(\mathrm{p},\alpha)^{24}\mathrm{Mg}$ measurements is divided between the experimental procedure and the procedure to measure a single energy point for clarity. Verification of the initial field settings of St. George was discussed in Section [REFERENCE] as is assumed for the remainder of this discussion.

4.3.1 Campaign Procedure

4.3.2 Run Procedure

At each energy point, preliminary runs were performed to verify the field settings of St. George and determine the systematic uncertainties of the tune. Following these checks, a final measurement at that energy was performed until the statistical uncertainty was below 1 % for on-resonance points and below 5 % for off-resonance points.

4.4 Data Reduction and Analysis

Each region of interest covered a single narrow resonance from the $^{27}\mathrm{Al}(\mathrm{p},\alpha)^{24}\mathrm{Mg}$ reaction. Extraction of resonance parameters from these regions required a data analysis pipeline to process the individual spectra from each strip of the Si detector and the detector spectra as a whole. Detection systematic uncertainties were determined individually for each energy measure prior to the final measurement at that energy. Target effects on the incident beam and produced α particles were explored [HOW?].

4.4.1 Experimental Systematics

The properties of the target, detector, and separator for the given experiment were explored through various means before, during, and after the data collection phase. Where applicable, the properties were compared to anticipated or predicted values. Differences between operating and testing conditions may be a cause of certain discrepancies within the detector spectra, as discussed below.

4.4.1.1 Target Properties

The self-supporting ^{27}Al target was measured to have a thickness of 62.50 $\pm$ 0.05 μg/cm^2. Target thickness was measured using an offline detector station with a ^{241}Am/^{148}Gd mixed α source. Runs with and without the target foil between the source and the detector lasted 600 s. The annular Si detector was not able to resolve the lowest intensity ^{241}Am peak during the runs, and only the highest intensity peak could be reliably resolved in the spectrum obtained with the target in place. The two spectra are shown in Fig. 4.1, and the α-particle peaks are given in Table 4.1.

The spectra were calibrated from the source-only run using the known energies of the emitted peaks. The shift in energy of the two largest peaks were recorded. The expected range for each peak was determined by interpolating the tabulated results from SRIM [12]. The target thickness was the difference in range for each peak between the degraded and undegraded α energies.

During the experiment, the total time of beam on target was minimized to limit the amount of carbon deposited on the target. Total charge accumulation on the order of 100 mC, with $\approx$ 75 mC from the final measurement runs. The longest measurement run deposited $\approx$ 25 mC on the target. At these levels, no appreciable change to the target thickness during the experiment could be seen. The target thickness was not remeasured following the end of the experimental campaign.

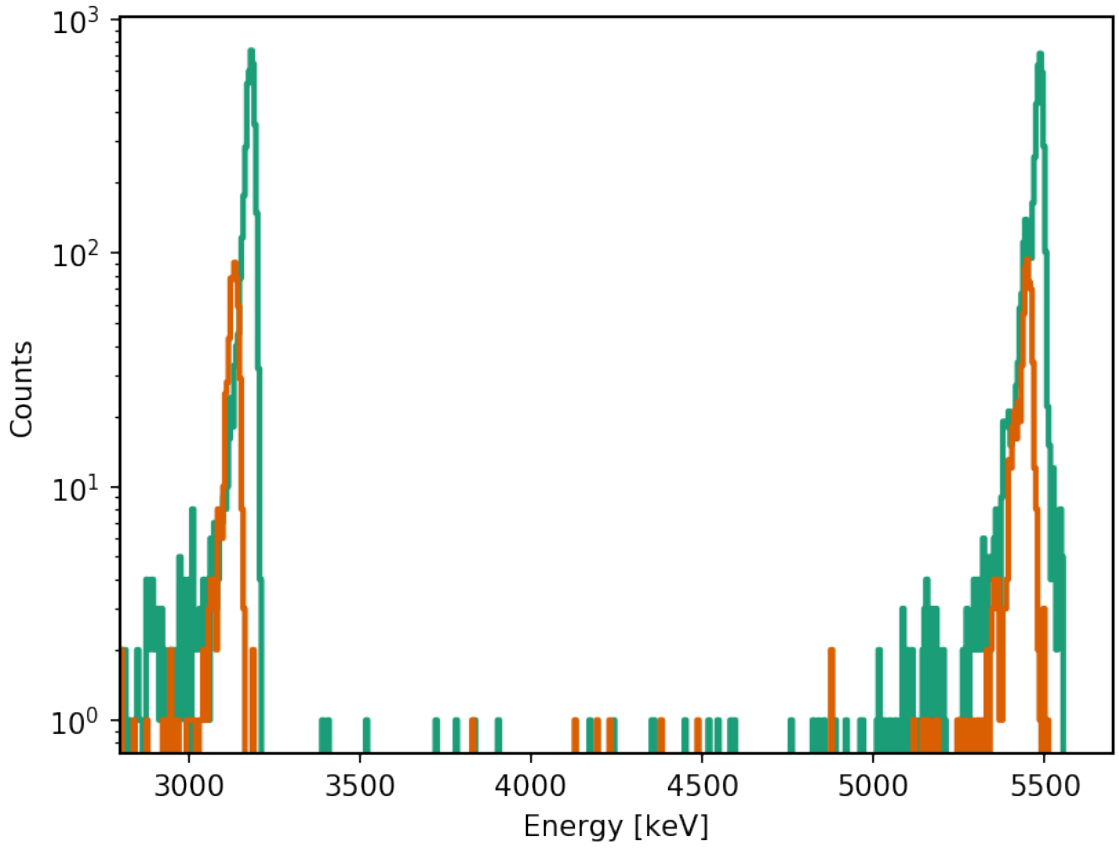

Figure 4.1. Target thickness measurement, showing the shift in the α peaks to lower energies due to the presence of the target. The initial spectrum is in green and the degraded spectrum is in orange. Only the energy range of interest is shown.

4.4.1.2 Detector Properties

The 16-strip Si detector was caibrated using a ^{241}Am/^{148}Gd mixed α source. Calibration runs were taken before and after the data collection phase, since the bias voltage was changed for the final runs. The final calibration run was taken with the same electronics setup and detector installation as during the run, except that the beam shield was removed.

Each strip and ADC were calibrated separately. A linear fit was used, as there only the two highest intensity α-particle peaks were resolved. Bins were shown to

TABLE 4.1

ALPHA PARTICLE ENERGIES FOR ^{241}Am/^{148}Gd MIXED SOURCE

Isotope	**E_α [keV]**	**Intensity**
^{148}Gd	3182.69	100 %
^{241}Am	5388	1.6 %
	5442.8	13.1 %
	5485.56	84.8 %

be approximately 2 keV for every strip. The resolution is cited for only the E_α = 3182.69 keV peak from ^{148}Gd as this is closer in energy to our expected particles. The calibration constants and detector resolutions are shown in Table 4.2.

The efficiencies of the individual strips were not determined and assumed to be 100 % for all. Measurements of similar detectors for the St. George detector system commissioning work showed > 99 % efficiencies across all strips.

The detector response shows low energy tails for both alpha peaks (see Fig. 4.2). The data show that the α events may fall outside of the two peaks. All events within our detector can then be considered real events, reducing the reliance on the energy calibration. The data also shows that the lower intensity ^{241}Am α peaks cannot be resolved.

4.4.1.3 Separator Properties

The energy resolving power is the minimum energy difference required to resolve a peak from the central image peak assuming that the change in energy is the only difference between the two peaks. By definition this quantity is only a first-order

TABLE 4.2

DETECTOR ENERGY CALIBRATION AND RESOLUTION

Strip	$\mathbf{a_0}$ **[keV]**	$\mathbf{a_1}$ **[keV/ch]**	**Resolution**
1	−85.61	1.6534	1.92 %
2	−165.12	1.7327	2.67 %
3	−123.66	1.5791	2.38 %
4	−172.41	1.6824	2.71 %
5	−194.53	1.6923	2.71 %
6	−235.36	1.7636	2.88 %
7	−202.59	1.7946	2.99 %
8	−203.93	1.8526	2.85 %
9	−269.19	1.8725	3.00 %
10	−252.46	1.8166	3.03 %
11	−243.02	1.8509	2.91 %
12	−272.25	1.8291	2.87 %
13	−235.06	1.8161	2.97 %
14	−172.81	1.7601	2.77 %
15	−235.26	1.8246	3.10 %
16	−110.00	1.6412	2.17 %

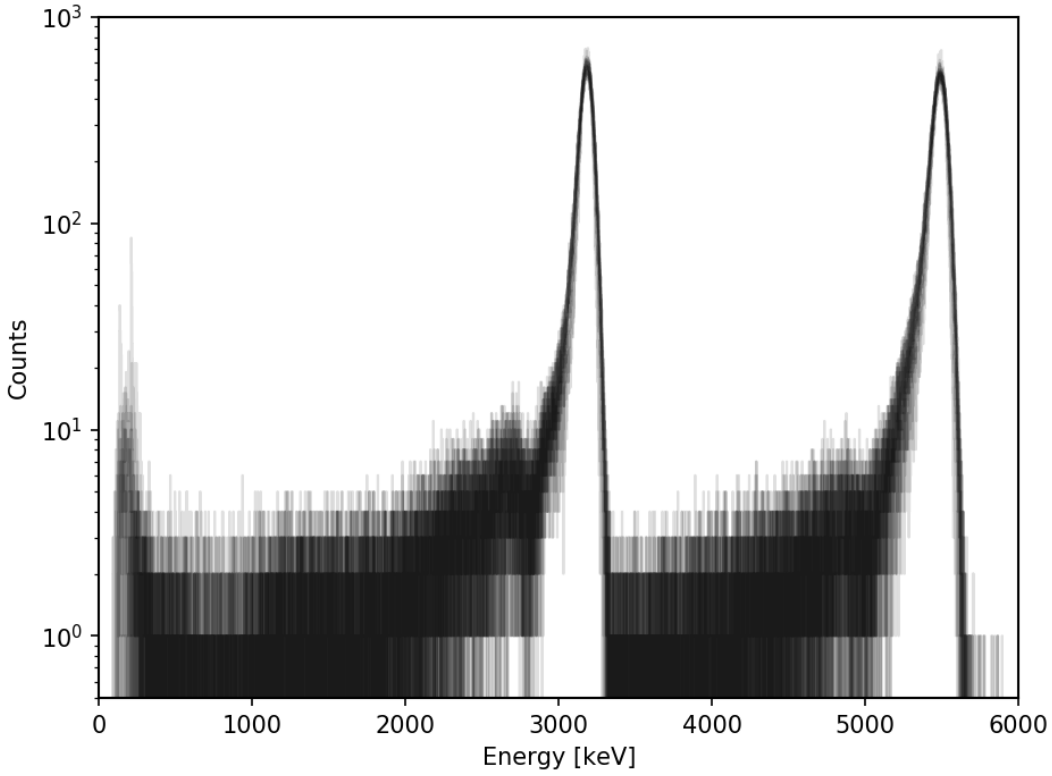

Figure 4.2. Example of the detector response from the energy calibration run. All 16 calibrated strips are overlayed to better show the overall trend. Long, low-energy tails from both calibration peaks can be seen. The counts in the lowest energy range are noise.

value, so only those parameters with a linear relationship with the position need be considered. The energy resolving power of the separator in relation to the terms present in the COSY transport map is defined as

$$\delta_k(\mathrm{RP}) \equiv \frac{2\left[(x|x)x_0 + (x|a)a_0\right]}{(x|\delta_k)}, \tag{4.1}$$

where x_0 and a_0 are the initial half-widths for position (in meters) and angle (in radians), respectively, and the remaining terms are the values from the transport map. The resolving power is only taken in the horizontal plane due to the vertical symmetry of the separator. The terms taken from the transport map are

$$(x|x) = 2.261610$$
$$(x|a) = -0.1368242$$
$$(x|\delta_k) = -0.2774295,$$

where signs are conserved for completeness. The maximal deviation caused by each terms is taken to be a positive value. The half-widths x_0 and a_0 are physically limited by the target chamber and taken to be $x_0 = 1.5$ mm and $a_0 = 42$ mrad, giving a resolving power of $\delta_k(\mathrm{RP}) = 0.286$. Since the produced α particles have an inherent spread in energy due to the incoming beam and the particles themselves interacting with the target, the energy resolution should be viewed as the window within which the energies are indistinguishable. As this window covers the expected energy spread of the produced α particles, there are no energy corrections required across the detector strips.

4.4.2 Yield Extraction

For each energy, the number of α-particle ejectiles produced was the total sum of counts within each detector strip above the maximum proton energy. Due to the detector response, any event above the noise threshold at ≈ 200 keV is a potential α event. There is still the possibility that some of the incident proton beam strikes the detector despite the rejection capabilities of St. George, so those counts below the maximum proton energy are rejected. The maximum proton energy is taken as the incident beam energy plus 3 % to be conservative. Since the proton beam is degraded in energy based on its interaction with the thin foil, this upper limit for the proton energy and lower limit for the α energy range will prevent any proton-induced counts from being counted. An example is shown in Fig. 4.3. While most runs did not show a discernible peak at the expected energy, this cut was still made. In those cases, "lost" counts were smaller than the statistical uncertainty of the counts above the energy threshold.

Beam currents at the target location were recorded before and after each run. For runs lasting longer than 15 m, the current was recorded every 15 m. The beam current was seen to fluctuate around the recorded value by up to 100 nA. For runs with multiple current readings, the average was taken as the nominal current. Time on target was recorded by the acquisition system.

The total yield for each energy is given by $Y(E) = N_r/N_b$, where N_r is the number of reaction products produced and N_b is the number of incident beam particles. If we include the detector and transport efficiency of our setup, and relate N_b to our incident beam current, our yield becomes

$$Y(E) = \frac{N_r}{\epsilon_d \epsilon_t I_b t}. \tag{4.2}$$

As our detector and transportation efficiencies are assumed to be 100 %, we can ignore

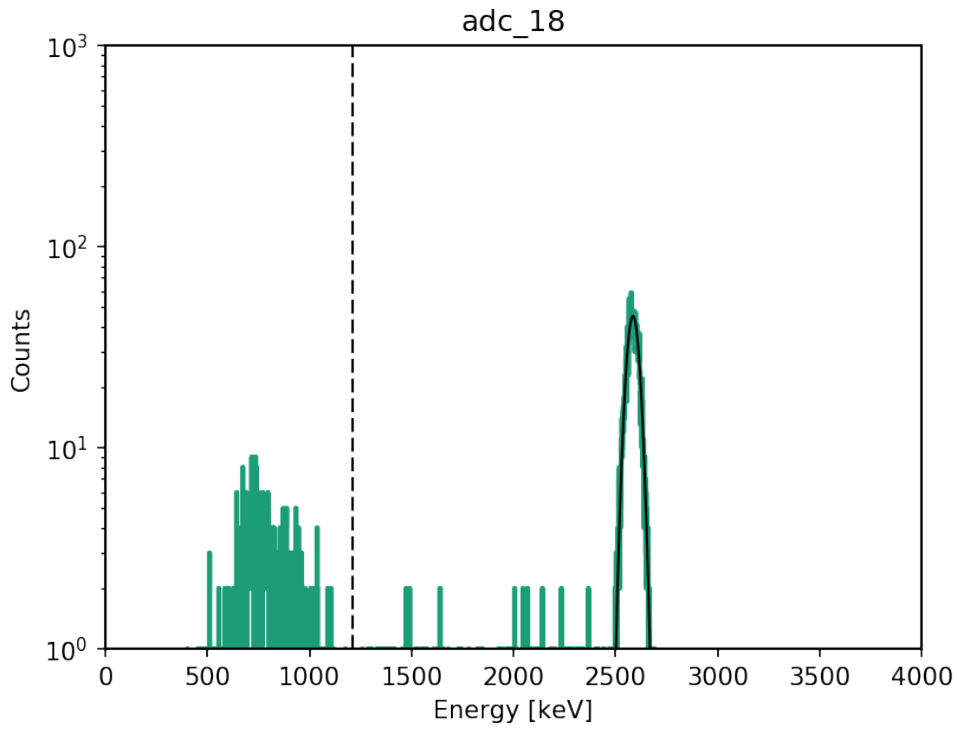

Figure 4.3. Possible proton peak within the spectrum of a single ADC. Data is from Run 241 ($E_{\mathrm{p}} = 1.1781$ MeV). The vertical dashed line shows the energy cut, with the potential beam peak below this energy. The remaining 15 strips for this run showed a similar peak in both central energy and counts.

those terms when calculating our yields.

Total uncertainty in the accumulated charge was on the order of $5 - 10\,\%$.

target

The mounted target is a 62.50 ± 0.05 μg/cm^2 self-supporting Al foil provided by Dr. Simon's group at the NSL. The target thickness was determined with a mixed ^{241}Am/^{148}Gd α source, providing α particles across the expected energy range, as shown in Table [REFERENCE]. Only the two highest intensity peaks in ^{241}Am could be reliably discriminated from the background, thus providing only three energy points for calibration purposes of the detector. Target thicknesses were measured using an offline setup, consisting of a Si detector within a vacuum chamber connected

to a data acquisition system. Data was recorded using MAESTRO for Windows [REFERENCE] and converted using `pyne`.

CHAPTER 5

RESULTS

CHAPTER 6

DISCUSSION AND CONCLUSION

APPENDIX A

POLE TIP FIELDS

For the two possible reaction study settings for St. George, the fields required are different. The difference arises from the difference in required recoil properties at the post-Wien filter focal plane F_2. The pole tip field settings for (α, γ) experiments are from using a mass $A = 41$ recoil in charge state $Q = 11^+$ with rigidities $B\rho =$ 0.331 Tm and $E\rho = 2.836$ MV (see Figure 3.1 for more details).

For the (p, α) experiment, the transported α particles have the properties listed in Table A.2. The incident proton beam is rejected within the COSY ion optics solution after the first dipole doublet B_1B_2, and the beam properties are not listed here.

TABLE A.1

POLE TIP FIELDS FOR (α, γ) AND (p, α) STUDIES

	Pole Tip Field [T]	
Quadrupole	(α, γ)	(p, α)
1	−0.163 032 76	−0.157
2	0.188 823 63	0.187
3	0.093 841 48	0.094 11
4	−0.126 204 02	−0.04
5	0.100 324 05	0.092
6	0.046 936 54	0.0585
7	0.0	−0.015
8	−0.097 791 79	
9	0.174 396 27	
10	0.210 922 28	
11	−0.139 623 55	

TABLE A.2

ALPHA PARTICLE PROPERTIES

Property [Unit]	**Value**
Energy [MeV]	2.504
ΔEnergy [%]	3
Angular spread [mrad]	40
Target diameter [mm]	3
Q [e]	2
$B\rho$ [Tm]	0.228
$E\rho$ [MV]	4.0

APPENDIX B

RUN INFORMATION

Additional information about the $^{27}\mathrm{Al}(\mathrm{p},\alpha)^{24}\mathrm{Mg}$ productions runs.

TABLE B.1

RUN ENERGY DETAILS

Run Numbers	**Field [G]**	E_p **[MeV]**	E_α **[MeV]**
261—264	1693.3	1.363 18	2.7700
265—270†	1690.4	1.358 52	2.7655
271—277	1687.1	1.353 22	2.7604
278—282	1683.9	1.348 09	2.7554
283—288	1680.1	1.342 01	2.7495
242—248	1580.8	1.188 07	2.5996
251—255	1577.5	1.183 11	2.5948
256—260†	1574.6	1.178 76	2.5905
229—234	1571.4	1.173 98	2.5859
235—241	1567.9	1.168 75	2.5808

†: Denotes runs at resonance energy

APPENDIX C

DEFLECTOR SETTINGS

Deflector settings used for commissioning work. Voltages are based on the physical characteristics of the deflector system and the beam properties to provide the necessary deflection. Setpoints are based on the version of the control program in place at the time of the experiments.

TABLE C.1

DEFLECTOR SETTINGS FOR TEST BEAMS

	$^{1}H^{+}$ at 1 MeV		$^{4}He^{+}$ at 2.3 MeV	
Angle [mrad]	**Voltage [kV]**	**Setpoint**	**Voltage [kV]**	**Setpoint**
5	0.363	9	0.834	24
10	0.725	20	1.668	49
15	1.087	31	2.501	74
20	1.450	42	3.335	100
25	1.813	53	4.170	125
30	2.176	64	5.004	150
35	2.539	75	5.839	175
40	2.902	86	6.674	201
45	3.265	97	7.509	226

APPENDIX D

ANALYSIS PACKAGE

During the course of the analysis work, two Python packages were developed to support the data conversion, storage, and analysis work: `pyne` and `sap`. These two packages were developed for Python 3.X using limited, standard scientific packages. Each of these packages will be discussed in turn, as well as justification behind developing them instead of using an established framework, such as ROOT[1].

D.1 Python for Nuclear Experiments

D.2 St. George Analysis Package

D.3 Justification

The `pyne` (Python for Nuclear Experiments) data framework is based on two main analysis codes and frameworks: the `ROOT` data analysis framework[2], and Dr. Karl Smith's `evt2root` conversion utility[2]. The `pyne` environment is designed to be similar to these packages, but since its development was alongside the analysis done for this experiment, additional functionality not needed for this analysis was not included. In particular, the buffer file processing only handles `.evt` and `.Chn` files, and the crate focus was on just a single ADC module. Additionally, most of the analysis work with these basic structures should be done using a separate package (such as the `sap` (St.

[1] `http://root.cern.ch/`

[2] `https://github.com/ksmith0/evt2root`

George Analysis Package)), and keeping the two responsibilities of data conversion and structure and analysis of said data results in cleaner code for the user.

Development of `pyne` started in March 2016, and the current version can be found on the package's GitHub page[3]. Within that same repository is the `sap` package, but that code is not reproduced here. The code listed is from version 0.6.0 (updated on May 12, 2017). The package outside of the standard library required for use is `numpy`, a standard numeric package for scientific python. Additional packages for `sap` are `scipy` (a scientific analysis package built on top of `numpy`) and `matplotlib` (a 2D plotting interface). Both are standards for scientific computing with python.

Currently, only Python 3.X is supported. As official support for Python 2.7 is set to terminate in 2020, and most scientific package managers have already switched to Python 3.X, this decision is warranted.

[3] `https://github.com/mmoran0032/pyne`

BIBLIOGRAPHY

1. R. Baartman and D. Kaltchev. *Proceedings of PAC2007*, pages 3229 – 3231, 2007. doi: 10.1109/PAC.2007.4440381.

2. R. Brun and F. Rademakers. Root - an object oriented data analysis framework, September 1996. URL `http://root.cern.ch/`.

3. M. Couder, G. P. A. Berg, J. Görres, P. J. LeBlanc, L. O. Lamm, E. Stech, M. Wiescher, and J. Hinnefeld. *Nuclear Instruments and Methods in Physics Research, Section A: Accelerators, Spectrometers, Detectors and Associated Equipment*, 587:35–45, Mar. 2008. doi: 10.1016/j.nima.2007.11.069.

4. G. Gilardy. Private communication, 2017.

5. E. Jones, T. Oliphant, P. Peterson, et al. SciPy: Open source scientific tools for Python, 2001–. URL `http://www.scipy.org/`. [Online; accessed 2017-03-29].

6. A. Kontos, D. Schrmann, C. Akers, M. Couder, J. Grres, D. Robertson, E. Stech, R. Talwar, and M. Wiescher. *Nuclear Instruments and Methods in Physics Research Section A: Accelerators, Spectrometers, Detectors and Associated Equipment*, 664(1):272 – 281, 2012. doi: https://doi.org/10.1016/j.nima.2011.10.039.

7. K. Makino and M. Berz. *Nuclear Instruments and Methods in Physics Research, Section A: Accelerators, Spectrometers, Detectors and Associated Equipment*, 558 (1):346–350, 3 2006. ISSN 0168-9002. doi: 10.1016/j.nima.2005.11.109.

8. Z. Meisel, K. Shi, A. Jemcov, and M. Couder. *Nuclear Instruments and Methods in Physics Research, Section A: Accelerators, Spectrometers, Detectors and Associated Equipment*, 828:8–14, 2016. doi: 10.1016/j.nima.2016.04.115.

9. Z. Meisel, M. T. Moran, G. Gilardy, J. Schmitt, C. Seymour, and M. Couder. *Nuclear Instruments and Methods in Physics Research Section A: Accelerators, Spectrometers, Detectors and Associated Equipment*, 850:48 – 53, 2017. doi: http://dx.doi.org/10.1016/j.nima.2017.01.035.

10. L. Morales, S. Kalkal, H. S. Jung, C. Seymour, G. Gilardy, M. Moran, Z. Meisel, J. Hinnefeld, and M. Couder. Performance of the st. george detector system. In *APS Division of Nuclear Physics Meeting Abstracts*, 2016. URL `http://meetings.aps.org/link/BAPS.2016.DNP.PC.7`.

11. J. A. Nelder and R. Mead. *The Computer Journal*, 7(4):308–313, 1965.

12. J. F. Ziegler, J. P. Biersack, and M. D. Ziegler. Srim-2008.04, 2008. URL `http://www.srim.org/`.